ZnSe Modified Zinc Metal Anodes: Toward Enhanced Zincophilicity and Ionic Diffusion

Tian Chen Li, Yew Von Lim, Xuesong Xie, Xue Liang Li, Guojing Li, Daliang Fang, Yifan Li, Yee Sin Ang, Lay Kee Ang, and Hui Ying Yang*

Zinc metal is an ideal candidate for aqueous rechargeable batteries due to its high theoretical capacity and natural abundance. However, its commercialization is inevitably challenged by several critical factors such as dendrite growth and parasitic side-reactions, leading to low coulombic efficiency and a limited lifespan. Herein, a modified Zn foil with a zincophilic ZnSe layer deposited by a simple selenization process is proposed. An order of magnitude stronger adsorption capability toward Zn^{2+} ions and uniform ion diffusion tunnels of ZnSe enables lower nucleation energy barrier and faster ion-diffusion kinetics. Meanwhile, detrimental Zn corrosion in aqueous system is also effectively mitigated. As a result, ZnSe@Zn anode shows reversible Zn plating/stripping (1700 h at 1 mA cm^{-2}) with ultra-low voltage hysteresis (41 mV), contributing to exceptional cycling stability over 500 cycles with negligible capacity fading for the $ZnSe@Zn/MnO_2$ full cell.

1. Introduction

With increasing environmental concerns, the demands for renewable energy have been rapidly growing in last decade.[1,2] Energy storage systems with eco-friendliness, cost-effectiveness, as well as safety features is highly desirable for sustainable energy solutions.[3–5] Recently, aqueous zinc-ion batteries have attracted extensive research attentions due to their distinctive
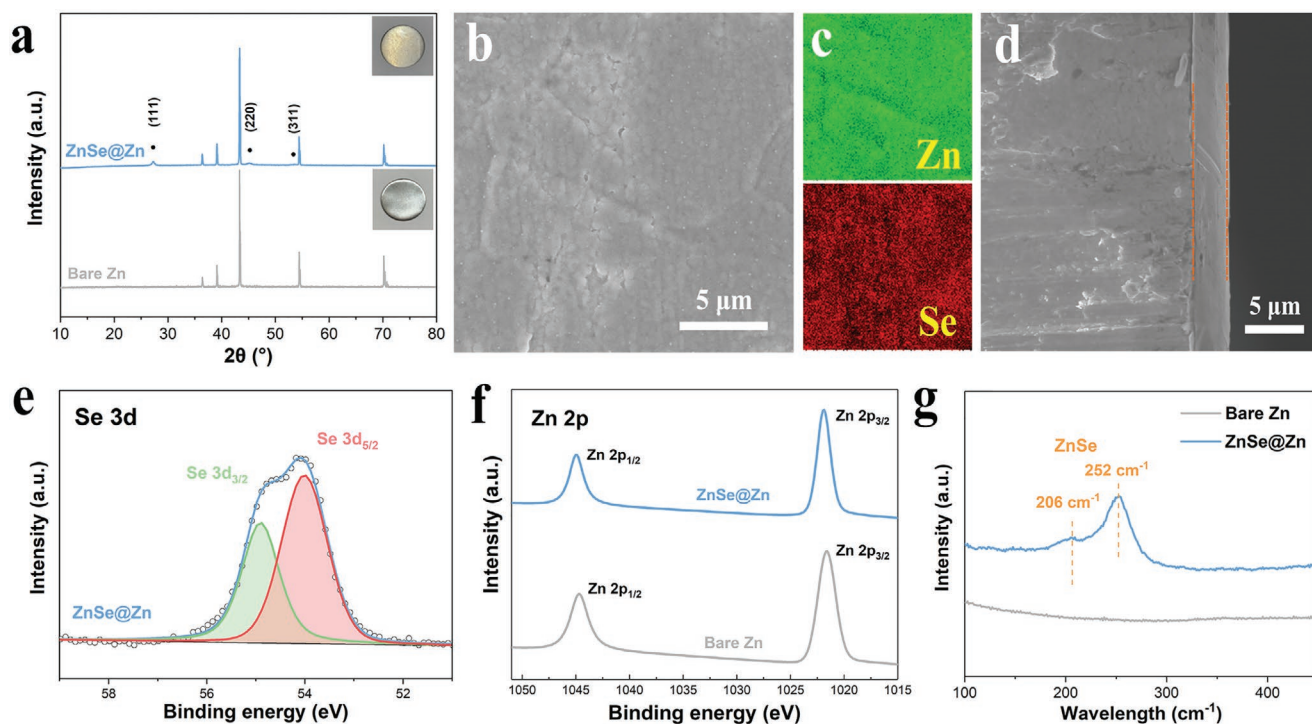
T. C. Li, Dr. Y. V. Lim, X. L. Li, Dr. D. Fang, Y. Li, H. Y. Yang
Pillar of Engineering Product Development
Singapore University of Technology and Design
8 Somapah Road, Singapore 487372, Singapore
E-mail: yanghuiying@sutd.edu.sg
X. Xie
School of Materials Science and Engineering
Central South University
Changsha 410083, P. R. China
Dr. G. Li
International Collaborative Laboratory of 2D Materials for
Optoelectronics Science and Technology of Ministry of Education
College of Optoelectronic Engineering
Shenzhen University
Shenzhen 518060, P. R. China
Prof. Y. S. Ang, Prof. L. K. Ang
Science
Mathematics and Technology
Singapore University of Technology and Design
Somapah Road, Singapore 487372, Singapore

merits, such as high theoretical capacity (820 mAh g^{-1}), low redox potential (–0.76 V vs SHE) and high natural abundance of zinc (Zn) metal anodes.[6,7] However, Zn in mildly acidic environment is plagued by dendritic growth, corrosion as well as hydrogen evolution, leading to a low coulombic efficiency and poor battery performance.[8,9]

Various solutions have been proposed, such as optimizing electrolytes,[10–12] designing flexible quasi-solid hydrogel,[13,14] adopting 3D current collectors,[15,16] and alloying tactics.[17,18] Among them, the introduction of artificial layer on Zn surface, namely surface modification, is most widely adopted due to its good practicability and effectiveness.[19,20] Kang et al. reported a $CaCO_3$ buffer layer to protect zinc anode. The nanoporous structure can guide Zn deposition and result in smooth plating surface.[21] Apart from the role in dendrite formation inhibition, the suppression of spontaneous side reactions can also be realized, such as $NaTi_2(PO_4)_3$ solid-state electrolyte layer,[22] pencil drawing interfacial layer,[23] and sieve-functional Kaolin layer.[24] However, these porous coatings have limited protection toward Zn surface due to the limitation of full isolation, resulting in severe safety concerns as well as high energy intake.[25] Furthermore, most protective layers realized by doctor-blading method suffer from poor bonding strength and localized inhomogeneities.[26,27] They are prone to peel off due to the repeated volume change during cycling. Therefore, developing a dense and structurally stable Zn-modified layer without significantly sacrificing ion conductivity is required.

Herein, unlike the traditional coating method (doctor blading for example) for Zn protection via mixing binder with designed materials, we develop a novel strategy to directly grow a uniform multi-functional ZnSe layer on the surface of Zn foil via a simple and facile selenization reaction. The resulted structure acts as a robust physical barrier and a highly zincophilic layer with ion-diffusion tunnels. The combination of the above merits enables stable electrochemical plating/stripping over 1700 cycles (1700 h) at 1 mA cm^{-2}, and ultra-low voltage hysteresis of 41 mV that outperforms most of the reported coating materials. Leveraging on this high reversibility and decreased nucleation energy barrier, $ZnSe@Zn/MnO_2$ batteries delivers initial capacity of 257 mAh g^{-1} and maintains ≈100% capacity retention after 500 cycles.

ADVANCED
SCIENCE NEWS
www.advancedsciencenews.com

NANO · MICRO
small
www.small-journal.com

Figure 1. a) XRD patterns and optical images of bare Zn and ZnSe@Zn. b) Top-view SEM image of ZnSe@Zn and c) corresponding EDS mapping of Zn and Se elements. d) Cross-sectional SEM images of ZnSe@Zn. High-resolution XPS spectra of e) Se 3d and f) Zn 2p for bare Zn and ZnSe@Zn. g) Raman spectra for bare Zn and ZnSe@Zn within the range 100–450 cm^{-1}.

2. Results and Discussions

The crystalline structure of Stilleite ZnSe consisted [ZnSe$_4$] stacks. Along the [110] direction, pyramidal [ZnSe$_4$] units exhibit an individual vertex-sharing chains array to form a tunnel structure with edge length of 4.01 Å, providing feasible diffusion paths for Zn^{2+} ions (0.75 Å) during the electrochemical process (Figure S1, Supporting Information).[28] In addition ZnSe is a wide-bandgap semiconductor (2.7 eV) and therefore suitable as electron-insulating layer to stabilize Zn anode.[29] Inspired by above merits, ZnSe was constructed on Zn surface via facile vapor–solid reaction method heating at optimized temperature of 250 °C (denoted as ZnSe@Zn). This served as an ion-guided layer to modulate the Zn^{2+} ion flux, and meanwhile play a role as a protective layer to avoid direct contact between the aqueous electrolyte and Zn surface.

Figure 1a shows typical X-ray diffraction (XRD) patterns of ZnSe@Zn. The peaks located at 27.2°, 45.2°, and 53.6° are well-indexed to the (111), (220), and (311) planes of ZnSe phase (PDF #04-5739), respectively. Surface and cross-sectional scanning electron microscope (SEM) images (Figure 1b,d) displays that the ZnSe layer is uniformly grown on Zn substrate with intimate contact, which can be confirmed by the homogeneous distribution of Se element from corresponding EDS mapping (Figure 1c and Figure S2, Supporting Information). In addition, the existence of ZnSe layer can be reflected by X-ray photoelectron spectroscopy (XPS) (Figure 1e,f). ZnSe@Zn exhibits two doublets belonged to Se 3d$_{3/2}$ and Se 3d$_{5/2}$, respectively, whereas no contribution is observed for Zn.[30] Moreover, there is a slight shift of Zn 2p signals after surface selenization.

This is mainly due to the changed coordination environment induced by the polar Zn—Se bond at the interface.[31] The formation of ZnSe modified layer was also characterized by Raman spectroscopy, where two new peaks centered at 206 and 252 cm^{-1} appear, corresponding to transverse optical (TO) and longitudinal optical (LO) phonon modes of ZnSe, respectively (Figure 1g).[32–34] Since the wettability of anode is directly relevant to the interfacial diffusion process, contact angle studies were investigated (Figure S3, Supporting Information). Compared with bare Zn, ZnSe@Zn features with smaller contact angle and better hydrophilicity, indicating easier access of zinc ions to anode surface.[35] Furthermore, the twisting experiment indicates good adhesion strength and structural integrity for ZnSe@Zn (Figure S4, Supporting Information). This can be explained by strong interfacial interaction between Se atoms from ZnSe layer and Zn atoms from Zn substrate.[36,37]

Apart from the ZnSe@Zn, the ZnSe layer synthesized at 300 and 350 °C (denoted as ZnSe@Zn-300 and ZnSe@Zn-350) were explored to evaluate the effect of reaction temperature on the growth. The typical peaks of ZnSe are observed in both XRD patterns and Raman spectra, demonstrating the same phase constitution between them (Figures S5 and S6, Supporting Information). SEM images shows that the thickness of ZnSe@Zn-300 layer is 20 µm, while ZnSe@Zn-350 surface layer is pulverized with a high thickness of 35 µm (Figure S7, Supporting Information). Moreover, the effect of reaction time was also investigated. The thickness of ZnSe layers increases when time is prolonged (Figure S8, Supporting Information). The thicker ZnSe layer inevitably suffers from structural instability and impeded interfacial ion transference, and
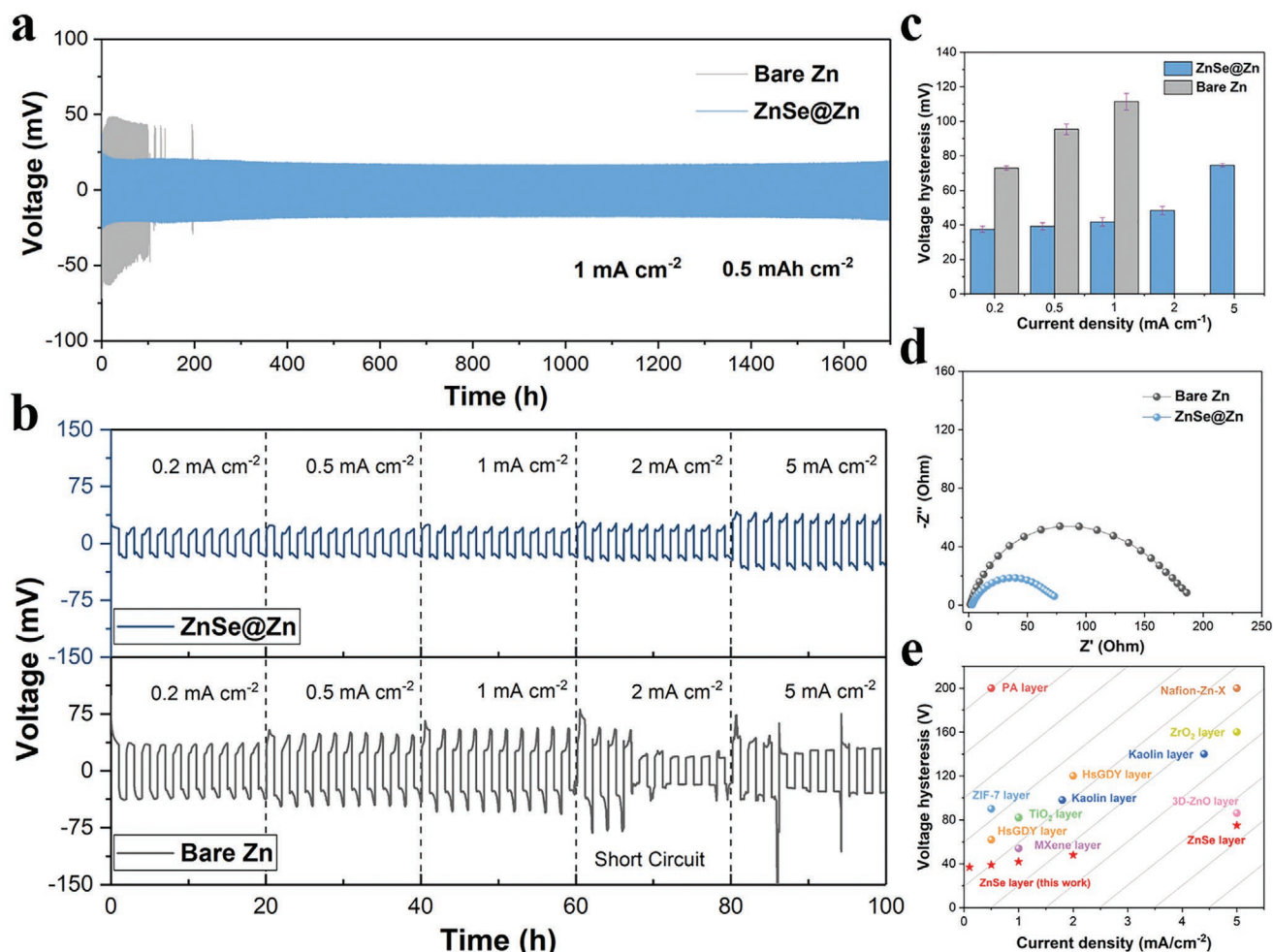
Figure 2. Comparison of electrochemical performance for symmetrical cells with bare Zn and ZnSe@Zn. a) Long-term galvanostatic cycling at a current density of 1 mA cm^{-2}. b) Rate performance and c) corresponding voltage hysteresis at various current densities from 0.2–5 mA cm^{-2}. d) Nyquist plots of symmetrical cells with bare Zn and ZnSe@Zn before cycling. e) Comparison of voltage hysteresis at different current densities between this work and the previously reported ones.

consequently results in poor reversibility, as verified by unstable voltage profile and limited cycling lifespan of symmetrical cells based on ZnSe@Zn-300 and ZnSe@Zn-350 (Figure S9, Supporting Information).

To confirm the feasibility of ZnSe layer in stabilizing Zn anode, the electrochemical behaviors of ZnSe@Zn were measured in a symmetric cell at current density of 1.0 mA cm^{-2} (**Figure 2**a). The bare Zn exhibits a fluctuating profile with a cycle life of 110 h. In contrast, reduced voltage hysteresis (41 mV) and enhanced cycling stability (>1700 h) are observed for ZnSe@Zn. In addition, the prolonged cycling lifespan (>1500 h) and lower voltage hysteresis (45 mV) of ZnSe@Zn versus bare Zn are realized at 2 mA cm^{-2} (Figure S10, Supporting Information). The improved cycling stability implies accelerated ion migration during the deposition/stripping process, which can be further evidenced by lower interfacial transfer resistance of cells with ZnSe@Zn before and after various cycles (Figure 2d; Figure S11, Supporting Information). The rate performance of symmetric cells was also investigated from 0.2 to 5 mA cm^{-2} (Figure 2b). The ZnSe@Zn cell

demonstrates lower polarization at various rates in comparison with the bare Zn cells. To be specific, the voltage hysteresis of ZnSe@Zn anode is 37, 39, 42, 48, and 74 mV at 0.2, 0.5, 1.0, 2.0, and 5.0 mA cm^{-2}, respectively, whereas the bare Zn cell exhibits a higher voltage hysteresis of 73, 95, and 111 mV at current densities from 0.2 to 1.0 mA^{-2} and deteriorates at 2 mA cm^{-2} after 66 h (Figure 2c). Such superior voltage hysteresis surpasses most of interfacial protective layer reported to date (Figure 2e; Table S1, Supporting Information).[24,26,38–44]

The significant performance improvement demonstrates that the dendrite issue plaguing zinc metal anodes has been effectively solved. To visually scrutinize this, the Zn plating process was monitored with in situ optical microscopy (**Figure 3**a). Uneven Zn plating with dendritic growth gradually appears on the surface of bare Zn with the increase of plating time, because Zn^{2+} is preferentially reduced at the irregular surface areas to minimize the surface energy ("tip effect").[45,46] The inhomogeneous Zn deposits are difficult to be fully stripped when discharged, resulting in impaired reversibility during repeated plating/stripping. In comparison, the ZnSe@Zn presents flat
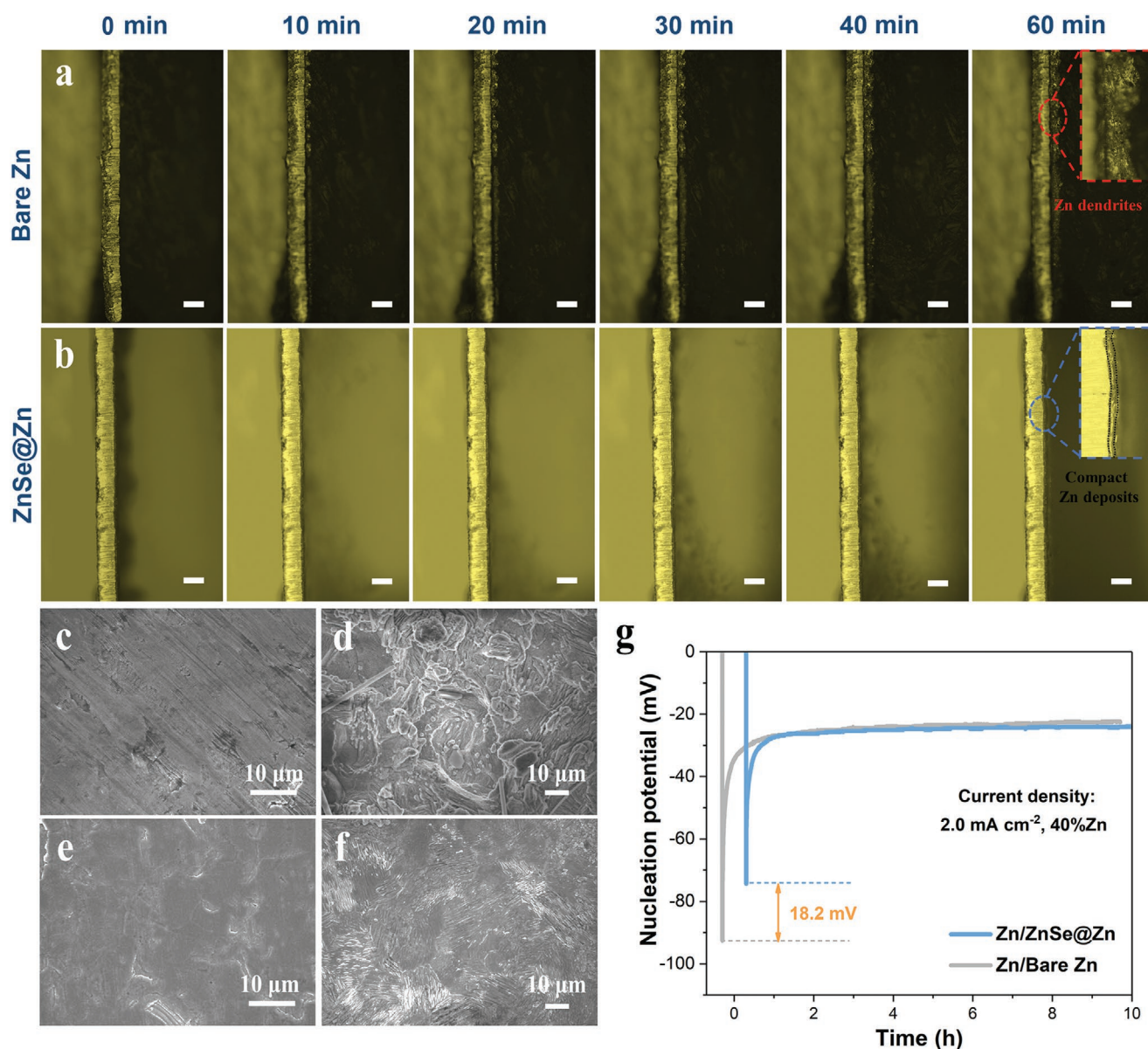
Figure 3. Optical micrographs of Zn deposition on a) bare Zn foil and b) ZnSe@Zn foil at different time points using in situ optical microscopy. Scale bar: 100 µm. SEM images of electrodes before and after cycling at 2 mA cm⁻² for 50 cycles, c,d) bare Zn, e,f) ZnSe@Zn. g) Nucleation overpotential of asymmetrical cells (vs Cu substrate).

plating surface. Even after plating for 60 min, the Zn deposits are compact with no dendritic tips emerged (Figure 3b). The regulated deposition pattern can also be validated by surface morphology of ZnSe@Zn after 50 cycles, where smoother plating surface is clearly observed compared with that of bare Zn (Figure 3c–f). Even after 200 cycles, ZnSe@Zn exhibits no Zn dendrite (Figure S12, Supporting Information). This indicates that the ZnSe modified layer still maintains its protective function during extended cycling.

Nucleation overpotential was subsequently examined to further investigate the impact of the ZnSe modified layer on Zn deposition. As shown in Figure 3g, ZnSe@Zn shows only 40.6 mV nucleation overpotential at the current density of 1 mA cm⁻², while the nucleation overpotential of bare Zn is 65.1 mV. Similar trend can also be found in Figure S13, Supporting Information, at various current density of 0.5, 2.0, and 5.0 mA cm⁻². Lower overpotential of ZnSe@Zn represents reduced nucleation energy barrier, leading to uniform distribution of Zn nucleation sites and dendrite-free Zn deposition.[41,47] To further affirm this, Cu electrodes stripped from asymmetrical cells with ZnSe@Zn and Zn anodes were compared after Zn deposition for various times (Figure S14, Supporting Information). It can be observed that Zn deposits are protruded in the Zn/Cu asymmetrical cell after 1 min plating. As the deposition time increases, the dendritic growth is aggravated. In comparison, spherical Zn deposits with dendrite-free surface morphology are observed in the ZnSe@Zn/Cu asymmetrical cell.[48] This finding suggests optimized nucleation

ADVANCED
SCIENCE NEWS
www.advancedsciencenews.com

NANO · MICRO
small
www.small-journal.com
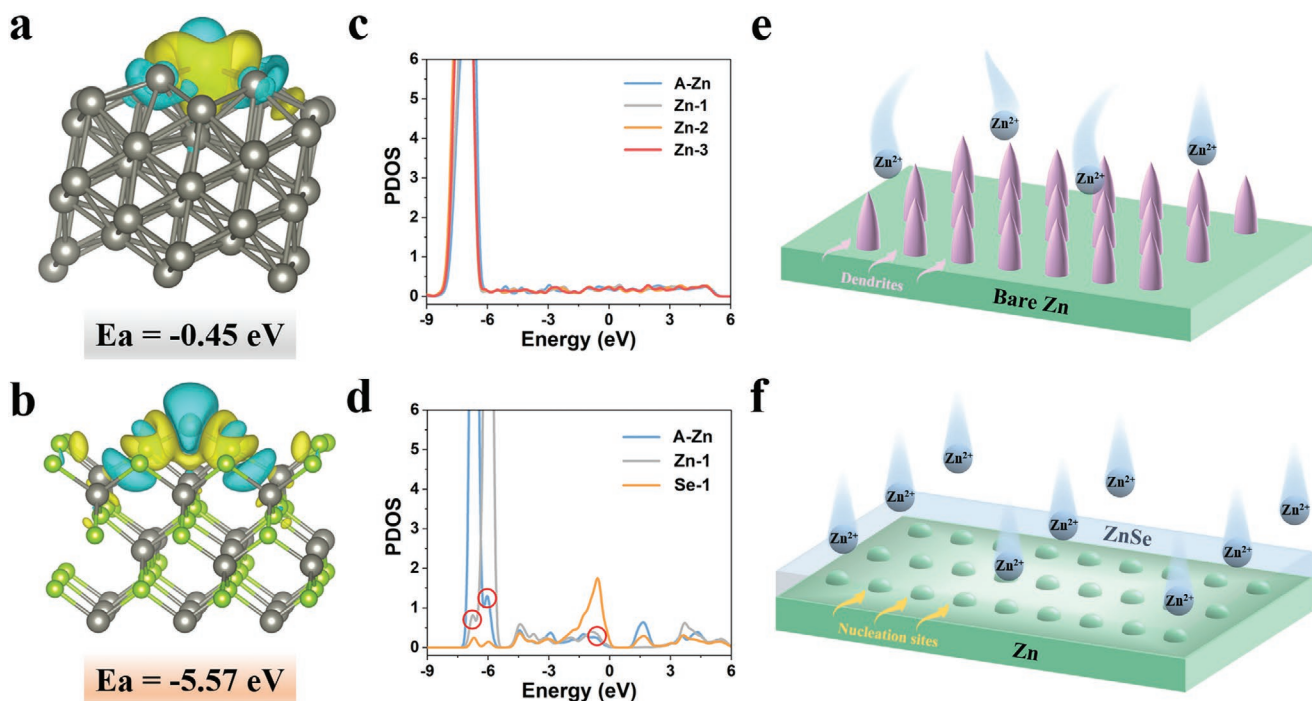
Figure 4. Charge density differences for the optimized structure of Zn^{2+} ion absorbed on a) Zn(111) and b) ZnSe(100) surfaces. The yellow and cyan regions represent charge accumulation and depletion, respectively. Partial density of states of c) bare Zn and d) ZnSe@Zn. Schematic illustration of Zn deposition on e) bare Zn and f) ZnSe@Zn.

process induced by ZnSe surface modification. Furthermore, the Zn deposition behavior can also be confirmed by chrono-amperometry (CA) characterization under a constant −150 mV potential (Figure S15, Supporting Information). As illustrated by the linear increase in current density, bare Zn exhibits irregular 2D diffusion mode, representing vertically accumulation on the protuberances with the lowest surface energy and ultimately form adverse Zn tips. In contrast, the ZnSe@Zn anode experiences a continuous 3D compact diffusion at ≈29 mA after a short 2D diffusion and nucleation process for 25 s, indicating uniform nucleation and almost unchangeable surface flatness during Zn plating.[43,49]

To uncover the positive effects of ZnSe layer on the interfacial ion diffusion and zinc nucleation at the atomic level, first principles' calculations based on density functional theory (DFT) were performed. The adsorption energy was investigated on the Zn^{2+} cation on various planes of ZnSe and Zn. ZnSe(100) and Zn(111) as the most representative surfaces were chosen for comparison, and their adsorption geometries are correspondingly constructed (Figure S16, Supporting Information). As displayed in **Figure 4**a,b, the differential charge densities exhibit that both substrates have chemical interaction with the divalent Zn^{2+} through Zn—Zn or Zn—Se bonds. The calculated adsorption energy of Zn^{2+} on the (100) surface of ZnSe is −5.57 eV, which is much higher than that of the (111) surface of Zn (−0.45 eV), suggesting better zincophilic ability of ZnSe than bare Zn. To reaffirm, partial density of states (PDOS) was evaluated (Figure 4c,d). The results demonstrate that electronic resonance from the peaks of adsorbed zinc ion (A-Zn) and the bonded Zn atom (Zn-1) for ZnSe(100), indicating strong inter-

action between the two atoms. As a comparison, there is no evident electron resonance peak for Zn(111). Similar trends can also be obtained from calculated adsorption energies and PDOS based on other facets of ZnSe and Zn (Figures S17 and S18, Supporting Information). As a result, this intrinsic affinity allows more zinc ions to diffuse through pyramidal [ZnSe4] ion tunnels with decreased energy barrier and form abundant nucleation sites, thus leading to more homogeneous Zn deposition resulting in the lack of obvious dendrite formation (Figure 4e,f).

In addition to the role of dendrite suppression induced by homogeneous nucleation, the anti-corrosion capability of designed ZnSe@Zn anode was also investigated. After soaking bare Zn into 2 M $ZnSO_4$ aqueous electrolyte for 5 days, there are many newly formed hexagonal flakes attached on the Zn surface, whereas clean surface of ZnSe@Zn is observed (Figure S19, Supporting Information). The strong peak within the orange area is confirmed to be $Zn_4SO_4(OH)_6 \cdot xH_2O$ by-products, as displayed as XRD patterns of bare Zn after soaking for 5 days (Figure S20, Supporting Information). In contrast, ZnSe@Zn shows significantly lower peak intensity of $Zn_4SO_4(OH)_6 \cdot xH_2O$, indicating mitigated side-reactions of the developed anode after modified with ZnSe. Moreover, linear polarization experiments were conducted to further evaluate the corrosion process. The ZnSe@Zn exhibits superior corrosion resistance, with lower exchange current (−2.69 mA) and more positive corrosion potential (−1.00 V) than bare Zn (Figure S21, Supporting Information). This is because the ZnSe layer strongly bonded with Zn serves as a physical barrier to isolate bulk electrolyte from Zn surface, thus inhibiting water-induced side-reactions.
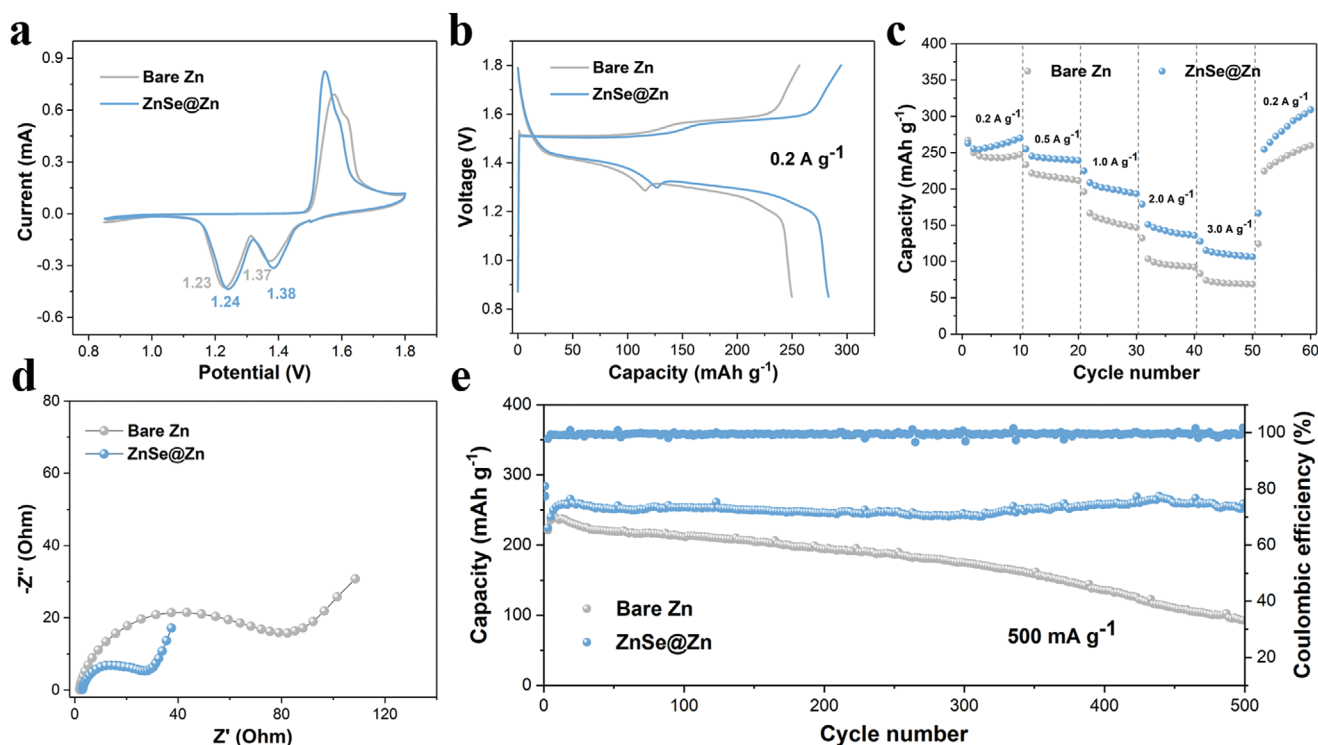
Figure 5. Comparison of the electrochemical performance of Zn/MnO$_2$ full batteries with bare Zn and ZnSe@Zn. a) CV profiles during the 2nd cycle. b) Typical charge/discharge curves at 0.2 A g^{-1}. c) Rate performance. d) EIS spectra before cycling. e) Long-term cycling performance at 500 mA g^{-1} of Zn foil/MnO$_2$ and ZnSe@Zn/MnO$_2$ batteries.

Full cells with MnO$_2$/CNT cathodes were assembled and tested to evaluate the practical applications of the ZnSe modified layer. The cathode material was synthesized by co-precipitation method (Figure S22, Supporting Information), and its XRD results displayed in the Figure S23, Supporting Information, is indexed to α-MnO$_2$ (PDF #44-0141).[22,44] The cyclic voltammetry (CV) curves of the bare Zn and ZnSe@Zn batteries were initially examined (**Figure 5**a and Figure S24, Supporting Information). The two pairs of redox peaks correspond to reversible Zn^{2+}/H$^+$ insertion/extraction reactions, which is consistent with the previously reported work.[50] Notably, the ZnSe@Zn battery exhibits higher exchange current and lower overpotential than the Zn counterpart during the first two cycle, indicating the enhanced redox kinetics contributed by ZnSe layer. As shown in the Figure 5b, the typical charge/discharge curves of the assembled ZnSe@Zn battery at 0.2 A g^{-1} shows narrower voltage gap than that of Zn-based battery. The rate performance of ZnSe@Zn/MnO$_2$ battery at various current densities from 0.2 to 3 A g^{-1} is displayed in Figure 5c and Figure S25, Supporting Information. Even at high rate of 3 A g^{-1}, the specific capacity of the ZnSe@Zn/MnO$_2$ battery retains 104 mAh g^{-1}, whereas that of Zn/MnO$_2$ battery is only 69 mAh g^{-1}. The inferior rate capability of the full cell assembled with bare Zn can be attributed to large charge transfer resistance and unfavorable ion migration behavior, which is verified by EIS results shown in the Figure 5d. In addition to the rate performance, the cycling stability of full cells was also examined. As demonstrated in Figure 5e, the capacity of Zn/MnO$_2$ battery remarkably drops to 93.5 mAh g^{-1} at 500 mA g^{-1} with 32.3% capacity

retention after 500 cycles. The capacity decay is mainly attributed to severe side-reactions occurring simultaneously, as well as the uncontrolled dendritic Zn growth during cycling. In contrast, owing to the superior Zn reversibility, the ZnSe@Zn/MnO$_2$ battery delivers initial capacity of 257 mAh g^{-1} after activation, and shows no obvious capacity loss after 500 cycles. Additionally, the superior cycling performance of the ZnSe@Zn battery at 1 A g^{-1} is indicated in Figure S26, Supporting Information, where 183.7 mAh g^{-1} is maintained after 800 cycles with a capacity retention of 93.2%.

3. Conclusion

In summary, a dense and stable ZnSe layer was designed and constructed on Zn anode via in situ facile selenization process. Benefited from excellent zincophilic ability and inherent ion-diffusion tunnels of ZnSe, fast ion transfer kinetics and uniform nucleation sites distribution can be realized for ZnSe@Zn. The symmetrical cells consequently exhibit favorable cycling stability (>1700 h) and exceptional rate performance at various depth of discharge from 0.2 to 5.0 mAh cm^{-2} with low voltage hysteresis, meanwhile the assembled ZnSe@Zn/MnO$_2$ full cells achieve long cycling life over 500 cycles with ≈100% initial capacity retained, resolving the impending issues in Zn anode in dendritic growth and inhibiting side reactions. This work provides a facile and cost-efficient strategy to stabilize Zn anode and holds great promise in developing advanced rechargeable Zn-based battery systems.

Supporting Information

Supporting Information is available from the Wiley Online Library or from the author.

Acknowledgements

Conflict of Interest

The authors declare no conflict of interest.

Data Availability Statement

Research data are not shared.

Keywords

[1] X. L. Li, T. C. Li, S. Huang, J. Zhang, M. E. Pam, H. Y. Yang, *ChemSusChem* **2020**, *13*, 1379.

[2] L. Guo, S. Vafakhah, M. Ding, M. E. Pam, Y. Wang, Y. Shang, S. Z. Huang, C. D. Gu, Y. Von Lim, H. Y. Yang, *Mater. Today Energy* **2020**, *16*, 100403.

[3] D. L. Chao, W. H. Zhou, F. X. Xie, C. Ye, H. Li, M. Jaroniec, S. Z. Qiao, *Sci. Adv.* **2020**, *6*, eaba4098.

[4] Y. Zhang, Z. Chen, H. Qiu, W. Yang, Z. Zhao, J. Zhao, G. Cui, *NPG Asia Mater.* **2020**, *12*, 4.

[5] T. J. Li, J. C. Sun, S. Z. Gao, B. Xiao, J. B. Cheng, Y. L. Zhou, X. Q. Sun, F. Y. Jiang, Z. H. Yan, S. L. Xiong, *Adv. Energy Mater.* **2021**, *11*, 2003699.

[6] C. Han, W. Li, H. K. Liu, S. Dou, J. Wang, *Nano Energy* **2020**, *74*, 104880.

[7] H. Jia, Z. Wang, B. Tawiah, Y. Wang, C.-Y. Chan, B. Fei, F. Pan, *Nano Energy* **2020**, *70*, 104523.

[8] T. T. Wang, C. P. Li, X. S. Xie, B. G. Lu, Z. X. He, S. Q. Liang, J. Zhou, *ACS Nano* **2020**, *14*, 16321.

[9] Q. Yang, Q. Li, Z. Liu, D. Wang, Y. Guo, X. Li, Y. Tang, H. Li, B. Dong, C. Zhi, *Adv. Mater.* **2020**, *32*, 2001854.

[10] L. S. Cao, D. Li, E. Y. Hu, J. J. Xu, T. Deng, L. Ma, Y. Wang, X. Q. Yang, C. S. Wang, *J. Am. Chem. Soc.* **2020**, *142*, 21404.

[11] N. N. Chang, T. Y. Li, R. Li, S. N. Wang, Y. B. Yin, H. M. Zhang, X. F. Li, *Energy Environ. Sci.* **2020**, *13*, 3527.

[12] T. S. Zhang, Y. Tang, S. Guo, X. X. Cao, A. Q. Pan, G. Z. Fang, J. Zhou, S. Q. Liang, *Energy Environ. Sci.* **2020**, *13*, 4625.

[13] Y. Tang, C. Liu, H. Zhu, X. Xie, J. Gao, C. Deng, M. Han, S. Liang, J. Zhou, *Energy Storage Mater.* **2020**, *27*, 109.

[14] M. Zhu, X. Wang, H. Tang, J. Wang, Q. Hao, L. Liu, Y. Li, K. Zhang, O. G. Schmidt, *Adv. Funct. Mater.* **2019**, *30*, 1907218.

[15] Y. Zeng, X. Zhang, R. Qin, X. Liu, P. Fang, D. Zheng, Y. Tong, X. Lu, *Adv. Mater.* **2019**, *31*, 1903675.

[16] C. Li, X. Shi, S. Liang, X. Ma, M. Han, X. Wu, J. Zhou, *Chem. Eng. J.* **2020**, *379*, 122248.

[17] S.-B. Wang, Q. Ran, R.-Q. Yao, H. Shi, Z. Wen, M. Zhao, X.-Y. Lang, Q. Jiang, *Nat. Commun.* **2020**, *11*, 1634.

[18] Z. Cai, Y. T. Ou, J. D. Wang, R. Xiao, L. Fu, Z. Yuan, R. M. Zhan, Y. M. Sun, *Energy Storage Mater.* **2020**, *27*, 205.

[19] J. N. Hao, X. L. Li, X. H. Zeng, D. Li, J. F. Mao, Z. P. Guo, *Energy Environ. Sci.* **2020**, *13*, 3917.

[20] W. C. Du, E. H. X. Ang, Y. Yang, Y. F. Zhang, M. H. Ye, C. C. Li, *Energy Environ. Sci.* **2020**, *13*, 3330.

[21] L. Kang, M. Cui, F. Jiang, Y. Gao, H. Luo, J. Liu, W. Liang, C. Zhi, *Adv. Energy Mater.* **2018**, *8*, 1801090.

[22] M. K. Liu, J. Y. Cai, H. S. Ao, Z. G. Hou, Y. C. Zhu, Y. T. Qian, *Adv. Funct. Mater.* **2020**, *30*, 2004885.

[23] Z. W. Li, L. Y. Wu, S. Y. Dong, T. Z. Xu, S. P. Li, Y. F. An, J. M. Jiang, X. G. Zhang, *Adv. Funct. Mater.* **2021**, *31*, 2006495.

[24] C. Deng, X. Xie, J. Han, Y. Tang, J. Gao, C. Liu, X. Shi, J. Zhou, S. Liang, *Adv. Funct. Mater.* **2020**, *30*, 2000599.

[25] L. Ma, M. A. Schroeder, O. Borodin, T. P. Pollard, M. S. Ding, C. S. Wang, K. Xu, *Nat. Energy* **2020**, *5*, 743.

[26] H. Yang, Z. Chang, Y. Qiao, H. Deng, X. Mu, P. He, H. Zhou, *Angew. Chem., Int. Ed.* **2020**, *59*, 9377.

[27] Z. H. Yi, G. Y. Chen, F. Hou, L. Q. Wang, J. Liang, *Adv. Energy Mater.* **2021**, *11*, 2003065.

[28] S. Y. Lu, T. X. Zhu, H. Wu, Y. K. Wang, J. Li, A. Abdelkaderkh, K. Xi, W. Wang, Y. G. Li, S. J. Ding, G. X. Gao, R. V. Kumarh, *Nano Energy* **2019**, *59*, 762.

[29] Q. Zhang, H. Q. Li, Y. Ma, T. Y. Zhai, *Prog. Mater. Sci.* **2016**, *83*, 472.

[30] Y. Y. He, L. Wang, C. F. Dong, C. C. Li, X. Y. Ding, Y. T. Qian, L. Q. Xu, *Energy Storage Mater.* **2019**, *23*, 35.

[31] J. N. Hao, B. Li, X. L. Li, X. H. Zeng, S. L. Zhang, F. H. Yang, S. L. Liu, D. Li, C. Wu, Z. P. Guo, *Adv. Mater.* **2020**, *32*, 2003021.

[32] H. L. Li, B. B. Wang, L. J. Li, *J. Alloys Compd.* **2010**, *506*, 327.

[33] E. Mosquera, N. Carvajal, M. Morel, C. Marin, *J. Lumin.* **2017**, *192*, 814.

[34] C. F. Dong, L. Q. Wu, Y. Y. He, Y. L. Zhou, X. P. Sun, W. Du, X. Q. Sun, L. Q. Xu, F. Y. Jiang, *Small* **2020**, *16*, 2004580.

[35] R. Yuksel, O. Buyukcakir, W. K. Seong, R. S. Ruoff, *Adv. Energy Mater.* **2020**, *10*, 1904215.

[36] L. Ma, Q. Li, Y. Ying, F. Ma, S. Chen, Y. Li, H. Huang, C. Zhi, *Adv. Mater.* **2021**, *33*, 2007406.

[37] J. N. Hao, J. Zhang, G. L. Xia, Y. J. Liu, Y. Zheng, W. C. Zhang, Y. B. Tang, W. K. Pang, Z. P. Guo, *ACS Nano* **2018**, *12*, 10430.

[38] Y. H. Cui, Q. H. Zhao, X. Wu, X. Chen, J. L. Yang, Y. T. Wang, R. Z. Qin, S. X. Ding, Y. L. Song, J. W. Wu, K. Yang, Z. J. Wang, Z. W. Mei, Z. B. Song, H. Wu, Z. Y. Jiang, G. Y. Qian, L. Y. Yang, F. Pan, *Angew. Chem., Int. Ed.* **2020**, *59*, 16594.

[39] Q. Yang, Y. Guo, B. Yan, C. Wang, Z. Liu, Z. Huang, Y. Wang, Y. Li, H. Li, L. Song, *Adv. Mater.* **2020**, *32*, 2001755.

[40] P. C. Liang, J. Yi, X. Y. Liu, K. Wu, Z. Wang, J. Cui, Y. Y. Liu, Y. G. Wang, Y. Y. Xia, J. J. Zhang, *Adv. Funct. Mater.* **2020**, *30*, 1908528.

[41] X. Xie, S. Liang, J. Gao, S. Guo, J. Guo, C. Wang, G. Xu, X. Wu, G. Chen, J. Zhou, *Energy Environ. Sci.* **2020**, *13*, 503.

[42] N. N. Zhang, S. Huang, Z. S. Yuan, J. C. Zhu, Z. F. Zhao, Z. Q. Niu, *Angew. Chem., Int. Ed.* **2021**, *60*, 2861.

[43] Z. M. Zhao, J. W. Zhao, Z. L. Hu, J. D. Li, J. J. Li, Y. J. Zhang, C. Wang, G. L. Cui, *Energy Environ. Sci.* **2019**, *12*, 1938.

[44] K. N. Zhao, C. X. Wang, Y. H. Yu, M. Y. Yan, Q. L. Wei, P. He, Y. F. Dong, Z. Y. Zhang, X. D. Wang, L. Q. Mai, *Adv. Mater. Interfaces* **2018**, *5*, 1800848.

[45] C. Xie, Y. Li, Q. Wang, D. Sun, Y. Tang, H. Wang, *Carbon Energy* **2020**, *2*, 540.

[46] Q. Li, Y. Zhao, F. Mo, D. Wang, Q. Yang, Z. Huang, G. Liang, A. Chen, C. Zhi, *EcoMat* **2020**, *2*, e12035.

[47] D. Kundu, S. H. Vajargah, L. W. Wan, B. Adams, D. Prendergast, L. F. Nazar, *Energy Environ. Sci.* **2018**, *11*, 881.

[48] J. N. Hao, L. B. Yuan, C. Ye, D. L. Chao, K. Davey, Z. P. Guo, S. Z. Qiao, *Angew. Chem., Int. Ed.* **2021**, *60*, 7366.

[49] R. Y. Wang, D. W. Kirk, G. X. Zhang, *J. Electrochem. Soc.* **2006**, *153*, C357.

[50] X. Gao, H. W. Wu, W. J. Li, Y. Tian, Y. Zhang, H. Wu, L. Yang, G. Q. Zou, H. S. Hou, X. B. Ji, *Small* **2020**, *16*, 1905842.